Engineering Chemistry
ISSN: 2813-6535, Vol. 11, pp 63-77
doi:10.4028/p-N7SbTD

Submitted: 2024-12-02
Revised: 2025-03-16
Accepted: 2025-03-21
Online: 2025-09-10

Synthesis, Structural, and Vibrational Properties of PVDF/$BiFeO_3$ Nanofibers using Electrospinning Technique

Faried Latief[1,a*], Putri Istichomah[2,b], Bagas Haqi Arrosyid[3,4,c], Ratih Amalia[3,d], Muhammad Fahroji[3,e], Trivadila[5,f], Akmal Zulfi[6,g], Andika Fajar[7,h], Andika Widya Pramono[1,i], and Alfian Noviyanto[3,8,j]

[1]Reseach Center for Advanced Materials, National Research and Innovation Agency (BRIN), Kawasan Puspiptek, Tangerang Selatan 15314, Banten, Indonesia

[2]College of Vocational Studies, IPB University, Jl. Kumbang No.14 Cilibende, Bogor, 16128, Indonesia

[3]Nano Center Indonesia, Jl. Puspiptek No.A-12 Setu, Tangerang Selatan, Banten 15314, Indonesia

[4]Department of Engineering Physics, Faculty of Industrial Technology, Institut Teknologi Bandung, Bandung 40132, Indonesia

[5]Department of Chemistry, Faculty of Mathematics and Natural Science, IPB University, Jl. Tanjung Kampus IPB Dramaga, Bogor 16680, Indonesia

[6]Research Center for Environmental and Clean Technology, National Research and Innovation Agency, Bandung 40135, Indonesia

[7]Research Center for Nanotechnology System, National Research and Innovation Council (BRIN), Kawasan Puspiptek, Tangerang Selatan 15314, Banten, Indonesia

[8]Departement of Mechanical Engineering, Mercu Buana University, Jl. Meruya Selatan Teknologi, Kebun Jeruk, Jakarta 11650, Indonesia

[b]istichomahputri@apps.ipb.ac.id, [c]bagashaqiarrosyid@nano.or.id, [d]ratih@nano.or.id, [e]fahroji@nano.or.id, [f]trivadila@apps.ipb.ac.id, [g]akmal.zulfi.m@brin.go.id, [h]andi009@brin.go.id [i]andi010@brin.go.id, [j*]a.noviyanto@nano.id and alfian.noviyanto@mercubuana.ac.id

Corresponding author: [a)*]fariedlatief@gmail.com

Keywords: Composite Nanofibers, PVDF/$BiFeO_3$, electrospinning, optimum formulation, energy storage materials.

Abstract. The composite nanofibers of PVDF/$BiFeO_3$ (PVDF/BF) signify a notable advancement in the domain of piezoelectric nanogenerators (PENGs), providing a high surface area alongside enhanced physicochemical properties for energy harvesting and storage applications. These nanofibers were synthesized through the electrospinning technique, which enables the creation of porous fibers by the dissolution of polymers in volatile solvents. This study investigates the crystalline and chemical structures of PVDF/BF nanofibers with modified formulations. X-ray diffraction (XRD) analysis has confirmed the presence of a rhombohedral (R3c) phase, characteristic of both $BiFeO_3$ and the PVDF phase. The measured fiber diameters for pure PVDF and PVDF/BF composites varied from approximately 400 nm to 950 nm. Fourier-transform infrared (FTIR) spectroscopy has identified absorption bands at 410–555 cm^{-1}, which correspond to the functional groups of $BiFeO_3$, as well as at 612–1430 cm^{-1} for PVDF. Moreover, Raman spectroscopy has validated molecular vibrational shifts for $BiFeO_3$ (4A1+9E) and PVDF within the range of 2973–2977 cm^{-1}. The incorporation of $BiFeO_3$ within the PVDF/BF nanofibers enhances the formation of the electroactive β-phase, thereby potentially improving their electrical properties.

Introduction

In recent years, the growing demand for sustainable and renewable energy sources has led to the exploration of innovative technologies [1,2]. There are several alternative energy sources**,** including solar energy materials (silicon, perovskite, and organic photovoltaic materials) [3–5], wind energy materials (steel, aluminum, and composite materials) [6], hydropower materials (concrete, steel, coating, and high-strength alloy) [7], geothermal energy materials (steel, high-temperature alloy, ceramic, and heat-resistance materials) [8], biomass and biofuel materials (organic materials and waste materials) [9,10], and piezoelectric materials (Bismuth ferrite (BF), and lead zirconate titanate (PZT), and nanomaterials) [11,12]. These materials represent how various energy technology pathways have been explored, offering cleaner and more sustainable future energy.

Piezoelectric materials are unique substances that generate electrical charges when subjected to mechanical stress, such as pressure, vibration, and bending. Their ability to transduce mechanical force into usable electricity has driven wide-used applications such as sensors, actuators, and energy-harvesting devices [13–15]. Recent progress in piezoelectric materials has led to the development of piezoelectric nanogenerators (PENGs). PENGs utilize piezoelectric materials at the nanoscale, which can convert mechanical energy from ambient vibrations, human movement, or other mechanical forces into electrical energy, making them ideal for powering small-scale electronic devices like sensors, wearable electronics, flexible and portable devices, or medical implants [16,17]. Since tunable microstructure holds a pivotal part in this field, the advancement of materials porosity becomes promising. One of them is the development of nanofibers PENGs which promotes unique advantages due to their high surface area and enhanced energy conversion efficiency [18,19].

The most common and versatile method in fabricating nanofibers is electrospinning**.** This technique allows to generate fibers at the nanoscale with controlled properties, including voltage, flow rate, humidity, and the distance between the syringe nozzle and the collector [20]. It involves the use of electrical forces to draw jet-formation from the needle to the collector. The immediate evaporation of solvent during the spinning process would frequently generate simultaneous amorphous and semi-crystalline materials. This typical morphology is further known in polycrystalline nanofibers (PNFs) that are particularly interesting due to their multiple crystalline grains, giving them distinct mechanical, electrical, and optical properties [21–23] for are beneficial in ceramics or metal oxide-based materials.

One of the well-established energy storage devices is bismuth ferrite ($BiFeO_3$)-based materials which have photovoltaic, photocatalytic, magnetic, and multiferroic (both ferromagnetic and ferroelectric) properties [24]. These promising features are owing to its electronic structure, where Bi^{3+} has $6s^2$ lone pair electrons, and is strongly hybridized with empty $6p^0$ orbital of Bi atom and $2p^6$ orbital of the O atom [25,26]. The main issues with $BiFeO_3$ include structural instability, mechanical fragility, short life cycles, and a lack of flexibility. Therefore, it is essential to obtain capacitors that offer high performance, energy density, and advanced stability, while also ensuring high sustainability and low-cost production. Notably, bismuth ferrite nanofibers have emerged as a highly effective material for piezoelectric applications, leveraging their significant sustainability and efficiency in mechanical energy harvesting, thus opening new possibilities for next-generation energy solutions.

Polyvinylidene fluoride (PVDF) is a piezoelectric polymer known for its flexibility and chemical resistance, commonly used in wearable sensors and flexible electronics. The β-phase of PVDF is the preferred phase that combines strong ferroelectric and piezoelectric properties [27]. Even though its piezoelectric effect is lower than ceramics, its considerable flexibility, lightweight properties, and high specific surface area are still worthwhile for the structural advancement [28]. The PVDF-$BiFeO_3$ composite nanofiber is expected to provide elastic interaction to the surface produced by the modifying agent, which can alter the spin structure of the $BiFeO_3$ magnetic field in

the interfacial region, leading to improved contact. The structural changes cause $BiFeO_3$ to exhibit alterations in the Fe-O-Fe bond angle of octahedral FeO_6, so the redistribution of charge and dipole orientation in the polymer matrix results in a higher coupling.

In this work, the PVDF/$BiFeO_3$ (PVDF/BF) composite nanofiber has been modified to optimize its structural and vibrational properties. The flexible polycrystalline nanofibers, composed of electrospun $BiFeO_3$ embedded in a PVDF polymer matrix through a sol-gel and electrospinning method, provide the ability to tune the electrical properties, durability, and morphology of materials.

Experimental

Synthesis

The $BiFeO_3$ (BF) powder materials are used in this study prepared by sol-gel auto combustion method by using Bismuth(III) nitrate ($Bi(NO_3)_3$) for analysis Merck (Cat. No. 1.01878.0100), Iron(III) nitrate nanohydrate ($Fe(NO_3)_3 \cdot 9H_2O$) Merck (Cat. No. 1.03883.0250), and Citric acid monohydrate ($C_6H_8O_7$) from SAP Chemicals (purity > 99.5%) [24,29]. This method merges the benefits of sol-gel processing and combustion synthesis, facilitating low-temperature fabrication and lower energy consumption compared to traditional methods. The sol-gel process begins with weighing metal precursors (Bismuth nitrate and Iron nitrate) and a chelating agent (Citric acid) according to stoichiometry at 0.02 mol. These components are then dissolved in deionized water to create a stable sol, which is subsequently transformed into a gel. Once the gel is formed, the auto-combustion process occurs. In this stage, the gel experiences spontaneous combustion due to the exothermic reaction between nitrates as oxidizers and citrate as fuel. [30]. Following the auto-combustion process, the $BiFeO_3$ powder undergoes purification and crystallization through calcination at a temperature of 600 ºC for 2 hours.

Fig. 1 displays the synthesis process from nanofiber PVDF/BF. The synthesized $BiFeO_3$ (BF) powder and Poly(vinylidene fluoride-co-hexafluoropropylene) (PVDF) polymer from Merck (CAS No. 9011-17-0) were weighed according to predefined ratios: 2.5 g of PVDF with 0 g of BF for pure PVDF, 1.250 g of PVDF with 1.250 g of BF for a 50% PVDF, 50% BF or PVDF/BF (50:50) composition, and 0.825 g of PVDF with 1.650 g of BF for a 33.33% PVDF, 66.67% BF or PVDF/BF (33:66) composition. DMAc was added in an amount of 5 mL and then placed into a 10 mL beaker. The PVDF powder was dissolved by gradually pouring it into the beaker containing DMAc [31]. After PVDF dissolved, $BiFeO_3$ material and 3.5 mL of DMAc were added and then re-dissolved for approximately 16 hours. The polymer dissolution process was conducted at a stirring speed of 300 rpm and a heating temperature of 50 ℃. The next step was the electrospinning process, where the polymer solution was placed in a syringe and extruded through a small needle under the influence of a high-voltage electric field at 15 kV with a 15 cm distance. [32,33]. The applied voltage will cause the polymer solution to form jets, forming a fine network that dries and collects as nanofibers. A Taylor cone forms according to the applied voltage [34]. The cone shape can last as long as the solution supply, surface tension, and viscosity are all stable.

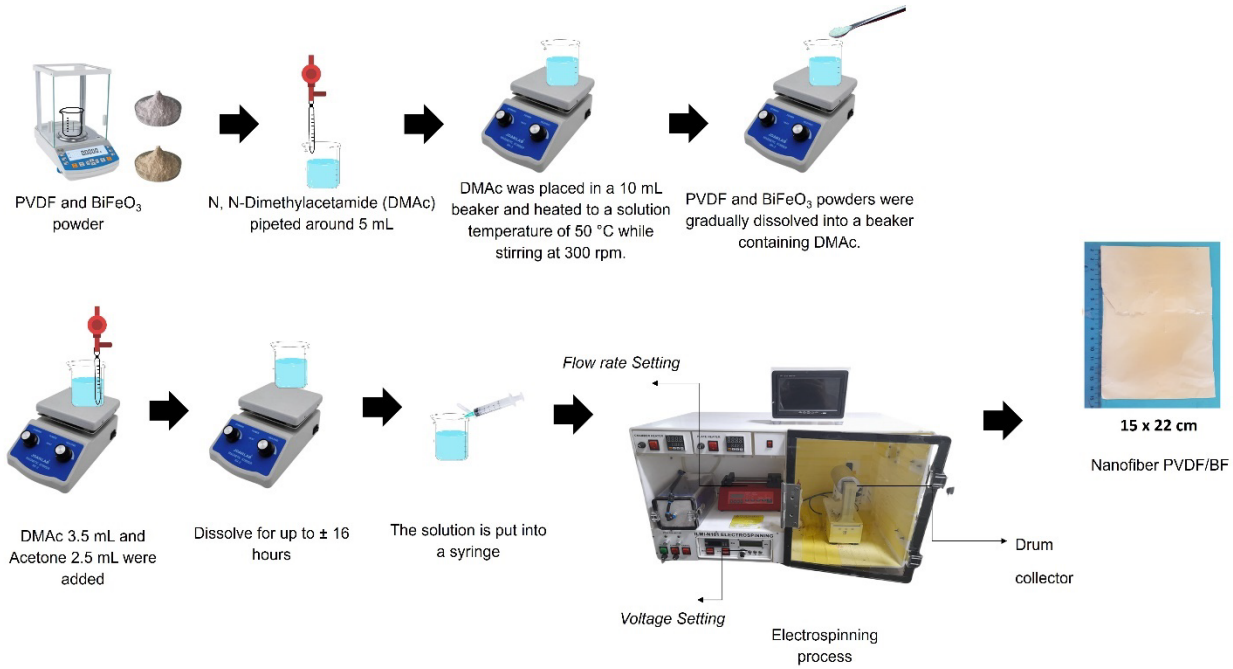

Fig. 1. Synthesis process from PVDF/BF nanofiber using electrospinning process.

Material Characterization

The particle size was measured using a Particle Size Analyzer (PSA) (Zetasizer Pro (ZSU 2300), Malvern, England). The crystalline structure and phase identification of the composite PVDF/$BiFeO_3$ nanofiber were recorded via X-ray Diffraction (XRD) with a Cu Kα source (Bruker D8 Advance 3Kw). Additionally, molecular vibrations were examined using a Fourier Transform Infrared Spectrometer (FTIR) (NicoletTM FTIR Spectrophotometer), as well as Raman spectra and Raman microscopy, which were recorded at room temperature with Raman spectroscopy (DXR3xi ThermoFisher Scientific).

Results and Discussion

Synthesis Nanofibers

Fig. 2 illustrates the physical appearance of the resulting nanofibers. The nanofibers formed from each formulation show an increase in brown color concentration from pure PVDF nanofiber (**Fig. 2.a**) to PVDF/BF (50:50) (**Fig. 2.b**). This increase is associated with the addition of BF material, which enhances the color intensity in the resulting nanofibers. Qualitative observations of this color can serve as a preliminary analysis of the optimal ratio of BF materials that can be composited with PVDF polymers. The formulations for pure PVDF and PVDF/BF (50:50) remain homogeneous and stable throughout the ten-hour electrospinning process. However, the visual appearance of the nanofibers indicates a reduction in color intensity over time. The nanofiber formulation for PVDF/BF (33:66) (**Fig. 2.c**) yields a pinkish-white color similar to that of pure PVDF nanofibers. This suggests that the incorporation of $BiFeO_3$ into the polymer matrix during nanofiber formation is not yet optimal. Despite the brown color of the solution, it is visually inferred that the optimal formulation is PVDF/BF (50:50).

In the PVDF/BF (33:66) formulation, the nanofiber solution could not be perfectly mixed, indicating inhomogeneity when there is a significant increase in the amount of material added [35]. The nanofiber solution in the PVDF/BF (33:66) formulation also shows a decrease in viscosity with the addition of BF material. This results in a thinner solution compared to pure PVDF and PVDF/BF (50:50). The outcomes of the electrospinning process heavily depend on the conditions of the prepared solution [36]. The solution must consider several factors, such as polymer concentration, viscosity, solvent type, and structure [37]. Low polymer concentrations result in sparsely distributed molecules in the solvent, leading to low viscosity of the solution. This causes the formation of an

unstable polymer network and results in smaller fibers with many beads. In contrast, PVDF/BF (50:50) produces fibers with a more uniform diameter and smooth morphology without beads. Meanwhile, at high concentrations, the viscosity of the solution becomes significantly high, leading to substantial steric hindrance, which further restricts the molecules' ability to move freely [38]. Inhomogeneous material particles will create aggregates, disrupting the uniform distribution of the polymer solution and potentially impacting the morphology of the nanofibers.

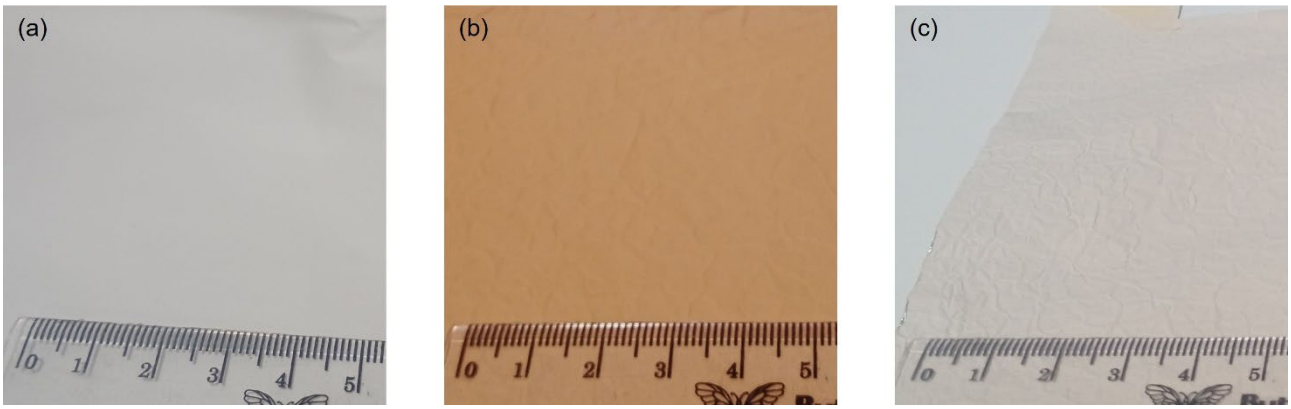

Fig.2. The PVDF/BF nanofibers result from the electrospinning process (a) PVDF, (b) PVDF/BF (50:50), (c) PVDF/BF (33:66) with the scale in centimeter.

Crystalline Structure and Microstructure

The nanofiber samples were characterized using XRD, as shown in Fig. 3, which illustrates the characteristics of the $BiFeO_3$ crystal structure before and after being composited with a polymer matrix. The phase analysis was then compared with the Crystallography Open Database (COD) No. 210-2915 for the $BiFeO_3$ phase and the International Center for Diffraction Data (ICDD) No. 00-042-1650 for PVDF, indicating the successful synthesis of $BiFeO_3$ and nanofiber PVDF/BF. The resulting diffractogram demonstrates the presence of the rhombohedral structure (space group R3c), with rhombohedral as the primary phase from $BiFeO_3$ [39]. There are doublet peaks at the diffraction index (1 0 4) and (1 1 0) which are characteristic peaks of pure $BiFeO_3$ [24]. Small peaks associated with the secondary phases appear at the diffraction indices (1 2 1), (0 1 3), and (-1 2 1) for Bismuth Iron Oxide ($Bi_2Fe_4O_9$), Sillenite (Fe-bearing) ($Bi_{25}FeO_{40}$), and Bismite (Bi_2O_3). [40–42]. The $BiFeO_3$ phase shows in three main peaks 2θ including 31.727º; 32.046º; and 22.398º. In addition, there are also 2θ positions at 45.721º; 56.920º; 56.308º; 51.264º; 51.700º; 39.452º; and 38.909º. The secondary phase is Bismuth (Bi_2O_3) which appears 2θ positions at 27.392º; 33.259º; and 33.029°. Another minor phase is Sillenite (Fe-bearing) ($Bi_{25}FeO_{40}$) at 27.608º; 30.301º; and 32.793º, while Bismuth iron oxide ($Bi_2Fe_4O_9$) is identified at 2θ of 28.152º; 28.930º; and 14.727º.

Overall, there is no significant difference between the results of $BiFeO_3$ powder and composite PVDF/BF (50:50) nanofibers. The diffraction pattern of PVDF displays two broad peaks at 2θ ~ 18-20º, which correlate with the α-phase, β-phase, and γ-phase forms of PVDF [43,44]. Rietveld refinement was conducted on the XRD pattern of calcined BF powder to determine its unit cell structure and symmetry. The final fitting parameters obtained from the Rietveld refinement were Rp = 1.42, Rwp = 2.05, and GoF = 2.81, indicating a good fit between the experimental and calculated profiles. The lattice constants estimated from the refinement were a = 5.5810 Å and c = 13.8760 Å.

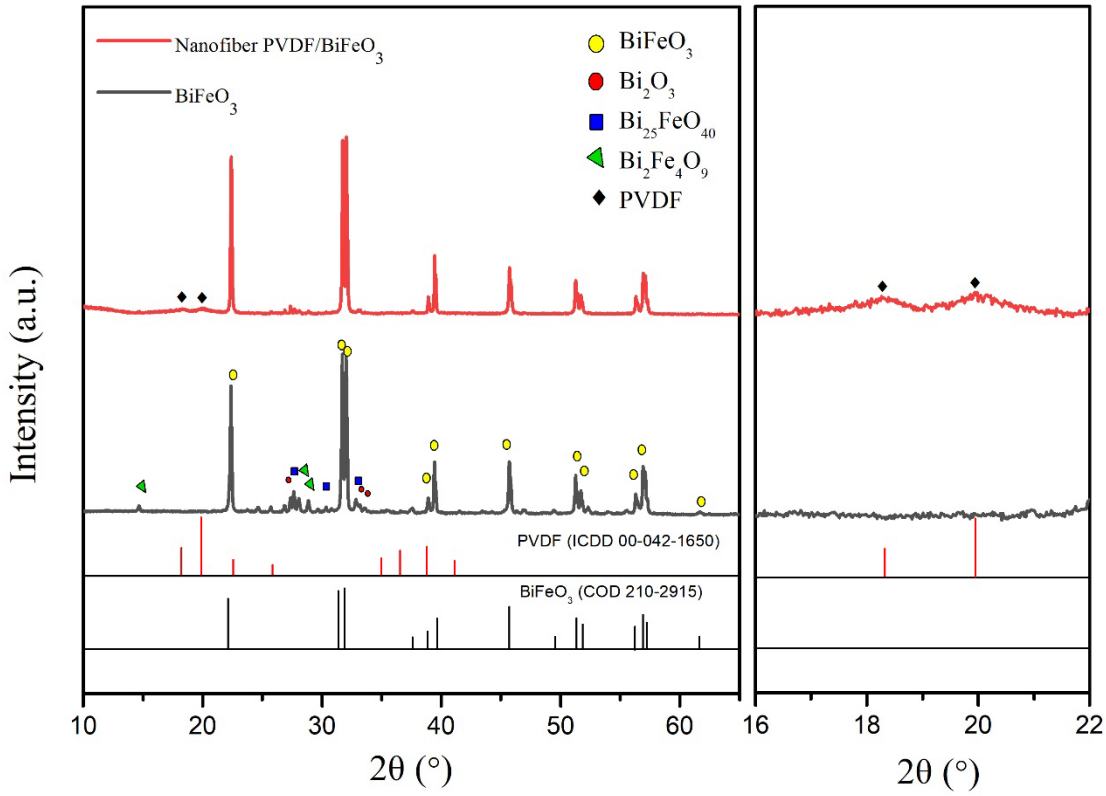

Fig. 3. XRD pattern from $BiFeO_3$ powder calcined at 600 ºC for 2h and composite PVDF/BF nanofiber. Insects clearly show the highest peak of PVDF in the range around 16°-22°.

PVDF/BF nanofibers typically exhibit a uniform fiber distribution with diverse orientations, which is commonly recognized as non-woven. This characteristic morphology of both pure PVDF and PVDF/BF nanofibers was analyzed using Raman microscopy. The resulting image facilitates the identification of individual fibers, enabling accurate fiber diameter measurements that are further analyzed using ImageJ software. Observation of nanofiber morphology was conducted by placing the nanofibers during the spinning process for 15 seconds, which were then observed at a magnification of 50x.

The morphology results of PVDF and PVDF/BF nanofibers are shown in Fig 4. Nanofibers were observed at a magnification of 50x. Based on visual observations, a nanofiber with a faint white color was obtained for the pure PVDF polymer. In contrast, PVDF/BF (50:50) and PVDF/BF (33:66) exhibited bead-like fibers. The measured fiber diameters for the pure PVDF and PVDF/BF (50:50) samples were 933 nm and 415 nm, respectively. The results indicate that increasing the material-to-polymer ratio in the nanofiber solution leads to a reduction in fiber diameter. However, for the PVDF/BF (33:66) formulation, fiber size could not be accurately observed due to the considerably high viscosity of the nanofiber solution, which was not fully dissolved. This likely obscured the jet formation during the spinning process. The instability of the PVDF/BF (33:66) solution is further evidenced by material sedimentation due to phase separation.

The fabrication of pure PVDF and PVDF/BF nanofibers was carried out using the same parameters for voltage control, flow rate, and needle-to-collector distance. Differences in the resulting fiber size may be attributed to the presence of side jets, which are affected by variations in the concentration of the nanofiber solution [45]. This aligns with the average measurements of PVDF/BF nanofibers, which exhibit a smaller fiber size due to the lower viscosity of the polymer solution used to produce pure PVDF. Solutions with low viscosity create beaded fibers because of insufficient polymer concentration in the precursor solution [46]. Solutions with low viscosity contain a greater

proportion of solvent molecules than polymer molecules, which makes solvent-intermolecular interactions more prevalent. When these solvent interactions are considerably stronger than charge interactions, polymer intermolecular forces, or polymer-solvent interactions, the polymer finds it difficult to move toward the collector, impeding fiber formation [47]. Furthermore, the fiber vibrational properties in PVDF, PVDF/BF (50:50) and PVDF/BF (33:66) are observed through Raman and FTIR as explained in the following paragraph.

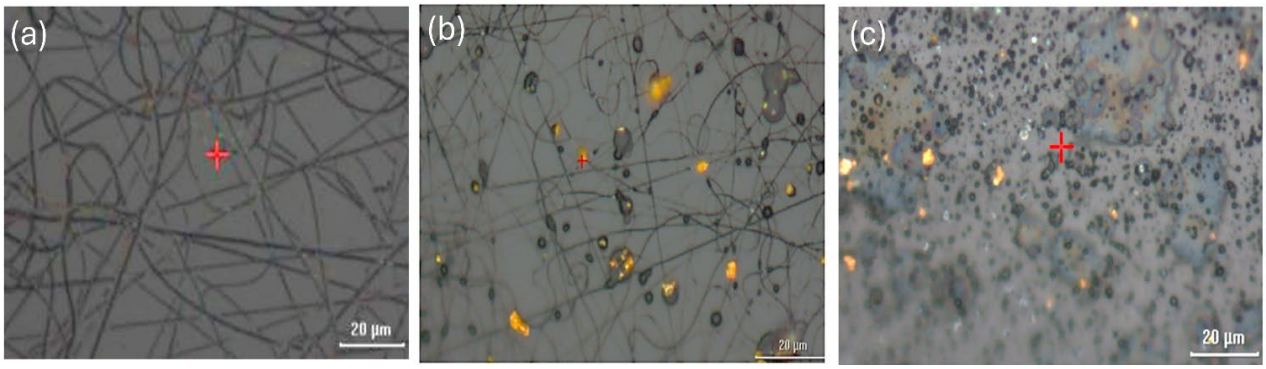

Fig. 4. Microstructure from fabricated nanofiber and composite nanofiber (a) PVDF, (b) PVDF/BF (50:50), and (c) PVDF/BF (33:66).

Vibrational Properties

To conduct a deeper analysis of the chemical structure in the composite PVDF/BF, characterization techniques such as Raman spectroscopy and FTIR are employed. **Fig. 5** displays the FTIR spectra of PVDF and the composite PVDF/BF nanofiber. The positions of the prominent characteristic bands in the spectra are listed in Table 1. PVDF polymer exhibits several different phases, including the α, β, and γ phases, each with distinct atomic arrangements and chain orientations. The chemical structure of PVDF can be represented as [-CH_2-CF_2-]n, where n denotes the number of repeating units in the polymer chain. The difluoromethylene (CF_2) and methylene (CH_2) functional groups were identified in the FTIR spectra of the nanofiber, indicating the properties derived from PVDF [38].

The vibrational peak at 1400 cm^{-1} corresponds to CF_2 symmetric stretching from the α-phase, while the peaks at 1174, 1175, 1177, and 1175 cm^{-1} represent the CF_2 symmetric group of difluoromethylene from the β-phase. The additional peaks at 1074 and 1073 cm^{-1} are associated with the stretching mode of the CF_2 asymmetric group from the β-phase. The next peak at 839 cm^{-1} reflects the transformation from the α-phase to the β-phase. The wave number peaks observed at 612 cm^{-1}, 761 cm^{-1}, and 796 cm^{-1} are present for both pure PVDF and PVDF/BF (50:50). Furthermore, the spectrum peaks at 613 cm^{-1}, 761 cm^{-1}, and 796 cm^{-1} for PVDF/BF (33:66) confirm the peaks of the α-phase from PVDF. More detailed peaks from the β-phase are also detected for pure PVDF at 511, 878, and 1276 cm^{-1}, PVDF/BF (50:50) at 509, 874, and 1275 cm^{-1}, and PVDF/BF (33:66) at 510, 877, and 1276 cm^{-1}, respectively. The last γ-phase was identified for pure PVDF, PVDF/BF (50:50), and PVDF/BF (33:66) as follows: 431 and 1430 cm^{-1}. Based on all these spectra, the presence of α, β, and γ phases is clearly identified in all samples, indicating that PVDF-based nanofibers have been successfully fabricated.

Typically, the absorption mode in the range below 1000 cm^{-1} is associated with the bond between inorganic elements [48]. This range of areas is evident with the addition of multiferroic materials like $BiFeO_3$, which can be observed from the presence of Fe-O and Bi-O groups primarily in PVDF/BF (50:50), identified at 410 cm^{-1} to 560 cm^{-1}. Additionally, the Bi-O stretching of BiO_6 was identified at 539 cm^{-1}, and the Fe-O of octahedral FeO_6 is reflected at 439 and 440 cm^{-1}. Other

Fe-O and Bi-O stretchings of BiO_6 and FeO_6 octahedra are prominently represented at 550, 555, 555, and 554 cm^{-1} in PVDF/BF (50:50), while their intensity is lower in PVDF/BF (33:66). This result suggests that the presence of $BiFeO_3$ is more pronounced at higher concentrations, reaching its optimal proportion at PVDF/BF (50:50). Meanwhile, the peak intensity between 600 cm^{-1} and 400 cm^{-1} is less pronounced compared to PVDF/BF (50:50) and is almost similar to that of pure PVDF, indicating that this formulation is less effective in dissolving BF into the PVDF matrix.

$BiFeO_3$ nanoparticles can interact with PVDF chains through physical or chemical bonds, changing the distribution of chain conformations and enhancing the formation of electroactive phases (β-phase and γ-phase) [49]. Conversely, the PVDF/BF (33:66) formulation experienced a decrease in the intensity of the FTIR results, which may be due to the fact that during the preparation of the PVDF/BF (33:66) nanofiber solution, $BiFeO_3$ materials could no longer be completely dissolved. Increasing the concentration of $BiFeO_3$ to an extreme level can disrupt solution stability and cause sedimentation, which leaves the pre-solution thinner. Higher concentrations of $BiFeO_3$ nanoparticles in PVDF/BF (33:66) can also lead to the formation of agglomerates, which reduce the homogeneity of the material and disrupt the distribution of the crystal phases in the nanofibers.

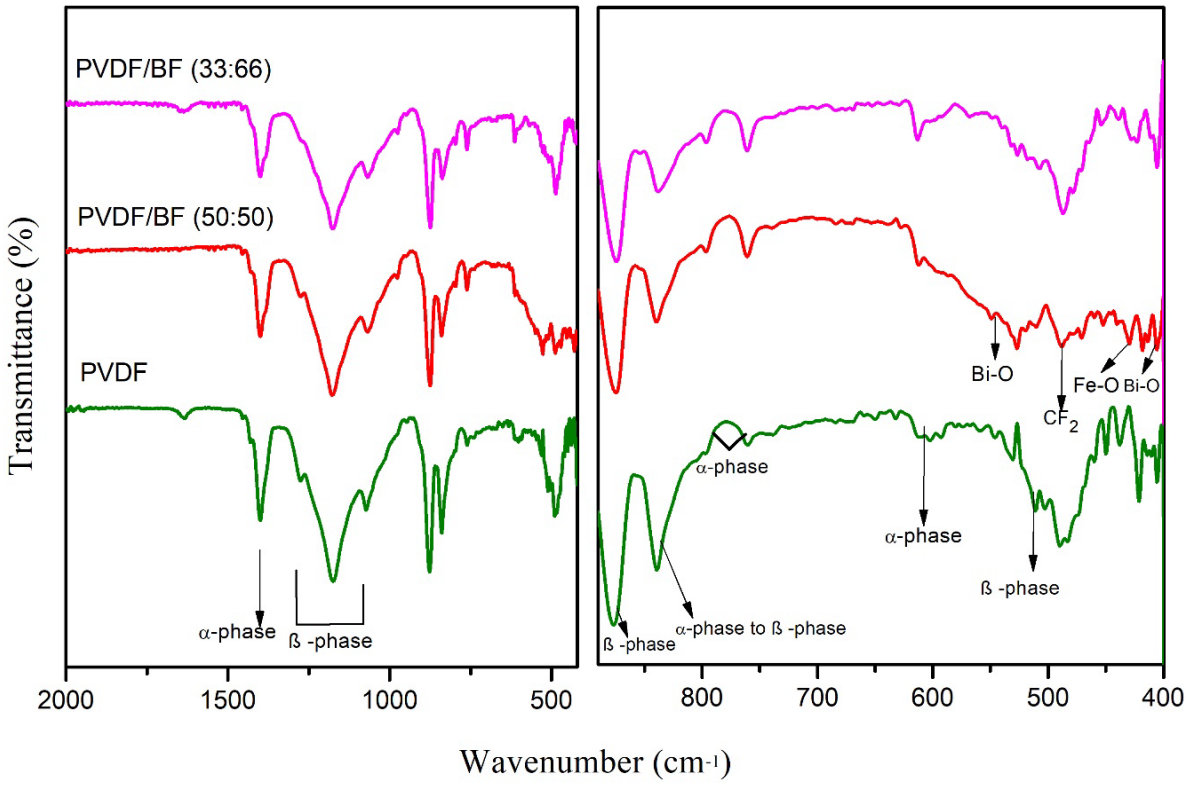

Fig. 5. FTIR spectra from fabricated nanofiber and composite nanofiber (a) PVDF, (b) PVDF/BF (50:50), and (PVDF/BF (33:66). Inset shows more detail the Bi-O and Fe-O bonding.

Table 1. FTIR band assignments of PVDF, PVDF/BF(50:50), and PVDF/BF(33:66) nanofiber.

No.	Wave number (cm^{-1})			References	Identification
	PVDF	PVDF/BF(50:50)	PVDF/BF(33:66)		
1.	-	413	411	410	Bending of Fe-O and Bi-O groups
2.	-	539	539	539	Bi-O stretching of BiO_6
3.	-	440	439	440	Fe-O of FeO_6 octahedral
4.	-	555	554	555	Fe-O and Bi-O stretching of BiO_6 and FeO_6 octahedral
5.	489	487	489	480 489	CF_2-bending and wagging α-phase
6.	612 761 796	612 761 796	612 761 796	614 763 795	α-phase
7.	839	839	839	840 1275	α-phase in raw powder converted into β-phase
8.	511 878 1276	510 875 1276	509 874 1276	511 840 1275	β-phase
9.	431 1430	431 1430	431 1430	431 1429	γ-phase
10.	1400	1400	1400	1406	CF_2 symmetric stretching, α-phase
11.	1175	1177	1175	1170	Symmetrical stretching of CF_2 group, β-phase
12.	1073	1073	1073	1073	Asymmetrical stretching of CF_2 group, β-phase

The Raman shift spectrum of PVDF/$BiFeO_3$ nanofibers was obtained using a laser power of 1.5 mW, an exposure time of 10 Hz, and a number of scans up to 500. The results are represented in **Fig. 6** and **Table 2**. The main peaks for each formulation in sequence for PVDF/BF (50:50) and PVDF/BF (33:66) were 2979, 2973, 2973, and 2977 cm^{-1}, which corresponded to the Raman spectrum of the polymer in its β-phase. The identified spectrum confirmed that there was more β-phase than α-phase due to the PVDF polymer used in the nanofiber manufacturing process. The spectrum of the pure γ phase at 1433 cm^{-1} was very strong, indicating that the main contribution to the peak at 1433 cm^{-1} arose from the γ phase. Notably, one of the strongest lines in the Raman spectrum of the α-phase at 796 cm^{-1} is only present as a shoulder in the spectrum that shows peaks at 835, 880, 1276, and 1433 cm^{-1} for the β-phase and γ-phase of PVDF. The presence of a strong Raman peak at 796 cm^{-1}, characteristic of the α-phase, appearing only as a shoulder in the spectrum with peaks at 835, 880, 1276, and 1433 cm^{-1}, suggests a phase conversion from α-phase to β-phase, along with the formation of the γ-phase in PVDF. This transformation is similar to that observed in the PVDF/ZnO system, where ZnO acts as a nucleating agent, facilitating an efficient phase transition from α-phase to β-phase, thereby enhancing piezoelectric properties [50,51]. A similar effect has been reported in the PVDF/PZT system, where PZT particles promote β-phase formation within the composite structure [52]. Furthermore, in the PVDF-TrFE/$BaTiO_3$ system, the addition of $BaTiO_3$ combined with a two-step poling method resulted in a high β-phase fraction in nanofiber samples [53].

Raman spectroscopy was also performed to identify the chemical structure of rhombohedral $BiFeO_3$ in PVDF/BF (50:50) and PVDF/BF (33:66), which exhibit R3c symmetry and comprise (4A1 + 9E) Raman active modes. These include 4 A1-symmetry longitudinal-optical (A1) optical modes and 8 E modes that represent the crystal characteristics of $BiFeO_3$ [48]**.** Modes E-1, A1-1, A1-2, A1-3, E-2, E-3, and E-5 closely align with the modes of the $BiFeO_3$ material structure. In contrast, E-2, A1-4, and E-4 show slight shifts, which are attributed to variations in material concentration. Raman spectra analysis indicates features below 400 cm^{-1} that represent Bi atoms in the perovskite structure,

while high-frequency vibrations above 400 cm^{-1} correspond to the stretching vibrations of octahedral Fe atoms (FeO_6). Three primary vibration modes at A1-1, A1-2, and A1-3 around the frequency bands of 135.15 cm^{-1}, 169.86 cm^{-1}, and 216–218 cm^{-1} signify the covalent bond between Bi and O, as well as the distortion caused by tetrahedral Bi atoms. The A1-4 vibration mode, located around 430−435 cm^{-1}, reflects the stretching vibrations of octahedral Fe atoms (FeO_6). The E vibration mode, occurring around 266−609 cm^{-1}, results from the distortion of octahedral FeO_6. [24].

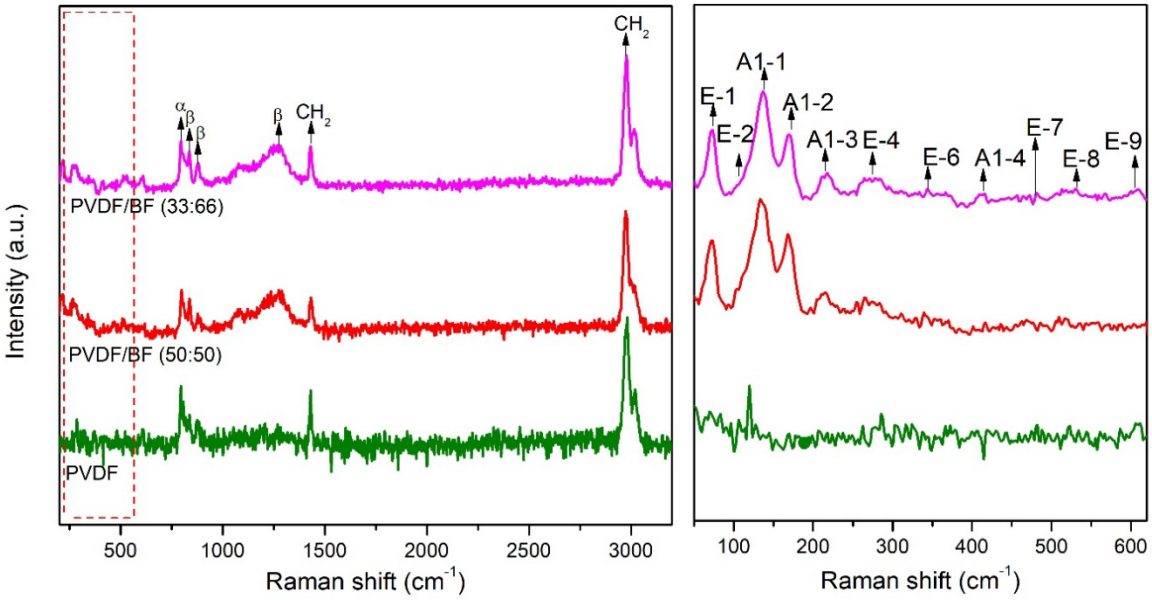

Fig. 6. Raman spectroscopy spectrum of PVDF, PVDF/BF (50:50), and PVDF/BF (33:66) nanofiber. The inset shows the Raman shift 50-610 cm^{-1}.

Table 2. Peak position of Raman active modes of PVDF, BF/PVDF(50:50), and BF/PDVF(33:66) nanofiber.

No.	Raman shift (cm^{-1})			References	Mode/Identification
	PVDF	PVDF/BF(50:50)	PVDF/BF(33:66)		
1.	-	73.44	73.44	72.95	E-1
2.	-	135.15	135.15	136.99	A_1-1
3.	-	169.86	169.86	169.31	A_1-2
4.	-	218.08	218.08	218.59	A_1-3
5.	-	266.89	277.86	266.23	E-4
6.	-	353.07	356.92	352.71	E-6
7.	-	432.13	435.99	428.84	A1-4
8.	-	115.87	115.87	115.88	E-2
9.	-	468.78	464.92	466.65	E-7
10.	-	526.83	530.00	528.00	E-8
11.	-	603.00	609.00	601.64	E-9
12.	796	798	796	799 795	α-phase
13.	880 1276	877 1274	880 1276	840 842 1278	β-phase
14.	1431	1433	1431	1433 1435	CH_2, (β-phase)
15.	2981	2973	2981	2974	CH_2 symmetric stretching (β-phase)

Conclusion

The nanofiber solution was successfully synthesized using the electrospinning method, incorporating various formulation variations: PVDF, PVDF/BF (50:50), and PVDF/BF (33:66). The measured fiber diameters for pure PVDF and PVDF/BF composites ranged from approximately 400 nm to 950 nm. Observing the physical appearance, PVDF/BF (50:50) shows a notable resemblance to the solution color and visually exhibits the highest homogeneity. Characterization of the PVDF/$BiFeO_3$ nanofibers was conducted using XRD, FTIR, and Raman spectroscopy, revealing the presence of α, β, and γ phases of the PVDF polymer, as well as the functional groups of the $BiFeO_3$ material. The potential dielectric properties are indicated by the results of nanofiber characterization using FTIR and Raman spectroscopy, which demonstrate the enhancement of functional groups and Raman shifts in the β and γ phases of the PVDF/BF nanofiber, along with the Bi-O and Fe-O functional groups.

Acknowledgements

This study was financially supported by the Center of Excellence Advanced Materials at Nano Center Indonesia. The authors would like to express their gratitude to Nano Center Indonesia for providing their facilities and characterization.

References

[1] K. Dissanayake, D. Kularatna-Abeywardana, A review of supercapacitors: Materials, technology, challenges, and renewable energy applications, Journal of Energy Storage 96 (2024) 112563. https://doi.org/10.1016/j.est.2024.112563.

[2] J. Zhang, Energy access challenge and the role of fossil fuels in meeting electricity demand: Promoting renewable energy capacity for sustainable development, Geoscience Frontiers 15 (2024) 101873. https://doi.org/10.1016/j.gsf.2024.101873.

[3] Y. Liu, Y. Xiao, J. Jia, H. Wang, W. Yan, M. Zhu, Perovskite solar cells: From planar designs to fiber-based innovations, Wearable Electronics 1 (2024) 150–159. https://doi.org/10.1016/j.wees.2024.07.004.

[4] K. Manwani, M. Lagier, A. Krammer, J. Fleury, A. Schüler, Development of novel orange colored photovoltaic modules with improved angular stability and high energy efficiency, Solar Energy Materials and Solar Cells 278 (2024) 113144. https://doi.org/10.1016/j.solmat.2024.113144.

[5] S. Wood, D. O'Connor, C.W. Jones, J.D. Claverley, J.C. Blakesley, C. Giusca, F.A. Castro, Transient photocurrent and photovoltage mapping for characterisation of defects in organic photovoltaics, Solar Energy Materials and Solar Cells 161 (2017) 89–95. https://doi.org/10.1016/j.solmat.2016.11.029.

[6] C. Li, J.M. Mogollón, A. Tukker, J. Dong, D. Von Terzi, C. Zhang, B. Steubing, Future material requirements for global sustainable offshore wind energy development, Renewable and Sustainable Energy Reviews 164 (2022) 112603. https://doi.org/10.1016/j.rser.2022.112603.

[7] E. Quaranta, P. Davies, Emerging and Innovative Materials for Hydropower Engineering Applications: Turbines, Bearings, Sealing, Dams and Waterways, and Ocean Power, Engineering 8 (2022) 148–158. https://doi.org/10.1016/j.eng.2021.06.025.

[8] F. Nath, M.N. Mahmood, E. Ofosu, A. Khanal, Enhanced geothermal systems: A critical review of recent advancements and future potential for clean energy production, Geoenergy Science and Engineering 243 (2024) 213370. https://doi.org/10.1016/j.geoen.2024.213370.

[9] Z.M.A. Bundhoo, R. Mohee, Ultrasound-assisted biological conversion of biomass and waste materials to biofuels: A review, Ultrasonics Sonochemistry 40 (2018) 298–313. https://doi.org/10.1016/j.ultsonch.2017.07.025.

[10] C. Chirat, Use of vegetal biomass for biofuels and bioenergy. Competition with the production of bioproducts and materials?, Comptes Rendus Physique 18 (2017) 462–468. https://doi.org/10.1016/j.crhy.2017.10.002.

[11] M. Absa, F. Latief, S. Suasmoro, Multistep sintering: its role on density, phase homogeneity, microstructure and electrical properties of (1-x-y)BaTiO3- xPbZrO3-yNaVO3 System, Journal of Physics (2020).

[12] T. Gholam, L.R. Zheng, J.O. Wang, H.J. Qian, R. Wu, H.-Q. Wang, Synchrotron X-ray Absorption Spectroscopy Study of Local Structure in Al-Doped BiFeO3 Powders, Nanoscale Res Lett 14 (2019) 137. https://doi.org/10.1186/s11671-019-2965-3.

[13] S. Banerjee, S. Bairagi, S. Wazed Ali, A critical review on lead-free hybrid materials for next generation piezoelectric energy harvesting and conversion, Ceramics International 47 (2021) 16402–16421. https://doi.org/10.1016/j.ceramint.2021.03.054.

[14] J. Rödel, K.G. Webber, R. Dittmer, W. Jo, M. Kimura, D. Damjanovic, Transferring lead-free piezoelectric ceramics into application, Journal of the European Ceramic Society 35 (2015) 1659–1681. https://doi.org/10.1016/j.jeurceramsoc.2014.12.013.

[15] W. Wang, X.-G. Tang, Y.-P. Jiang, Q.-X. Liu, W.-H. Li, X.-B. Guo, Z.-H. Tang, Phase evolution, dielectric, ferroelectric, and piezoelectric properties of Bi(Mg0.5Hf0.5)O3–modified BiFeO3–BaTiO3, Materials Today Chemistry 24 (2022) 100825. https://doi.org/10.1016/j.mtchem.2022.100825.

[16] M.H. Bagheri, A.A. Khan, S. Shahzadi, M.M. Rana, M.S. Hasan, D. Ban, Advancements and challenges in molecular/hybrid perovskites for piezoelectric nanogenerator application: A comprehensive review, Nano Energy 120 (2024) 109101. https://doi.org/10.1016/j.nanoen.2023.109101.

[17] S. Divya, T.H. Oh, M. Bodaghi, 1D nanomaterial based piezoelectric nanogenerators for self-powered biocompatible energy harvesters, European Polymer Journal 197 (2023) 112363. https://doi.org/10.1016/j.eurpolymj.2023.112363.

[18] A. Biswas, S. Garain, K. Maity, K. Henkel, D. Schmeißer, D. Mandal, Influence of *in situ* synthesized bismuth oxide nanostructures in self-poled PVDF-based nanogenerator for mechanical energy harvesting application, Polymer Composites 40 (2019). https://doi.org/10.1002/pc.24628.

[19] Z. Pourkarim, H. Esfahani, Enhancement of acoustic properties of carbon fibrous membrane (CFM) by in-situ crystallization of PZT nanogenerators (PENGs) inside the fibers for a low-frequency acoustic energy harvesting, Ceramics International 50 (2024) 25955–25968. https://doi.org/10.1016/j.ceramint.2024.04.338.

[20] A. Zulfi, M.M. Munir, D.A. Hapidin, A. Rajak, D. Edikresnha, F. Iskandar, K. Khairurrijal, Air filtration media from electrospun waste high-impact polystyrene fiber membrane, Mater. Res. Express 5 (2018) 035049. https://doi.org/10.1088/2053-1591/aab6ef.

[21] W. Fu, W. Xu, K. Yin, X. Meng, Y. Wen, L. Peng, M. Tang, L. Sun, Y. Sun, Y. Dai, Flexible-in-rigid polycrystalline titanium nanofibers: a toughening strategy from a macro-scale to a molecular-scale, Mater. Horiz. 10 (2023) 65–74. https://doi.org/10.1039/D2MH01255C.

[22] V. Kundrat, V. Vykoukal, Z. Moravec, L. Simonikova, K. Novotny, J. Pinkas, Preparation of polycrystalline tungsten nanofibers by needleless electrospinning, Journal of Alloys and Compounds 900 (2022) 163542. https://doi.org/10.1016/j.jallcom.2021.163542.

[23] G. Wang, Y. Ji, X. Huang, X. Yang, P.-I. Gouma, M. Dudley, Fabrication and Characterization of Polycrystalline WO 3 Nanofibers and Their Application for Ammonia Sensing, J. Phys. Chem. B 110 (2006) 23777–23782. https://doi.org/10.1021/jp0635819.

[24] D. Carranza-Celis, A. Cardona-Rodríguez, J. Narváez, O. Moscoso-Londono, D. Muraca, M. Knobel, N. Ornelas-Soto, A. Reiber, J.G. Ramírez, Control of Multiferroic properties in BiFeO3 nanoparticles, Sci Rep 9 (2019) 3182. https://doi.org/10.1038/s41598-019-39517-3.

[25] T. Durga Rao, S. Asthana, Evidence of improved ferroelectric phase stabilization in Nd and Sc co-substituted BiFeO3, Journal of Applied Physics 116 (2014) 164102. https://doi.org/10.1063/1.4898805.

[26] S. Shankar, I. Maurya, A. Raj, S. Singh, O.P. Thakur, M. Jayasimhadri, Dielectric and tunable ferroelectric properties in BiFeO3–BiCoO3–BaTiO3 ternary compound, Appl. Phys. A 126 (2020) 686. https://doi.org/10.1007/s00339-020-03872-0.

[27] R. Dallaev, T. Pisarenko, D. Sobola, F. Orudzhev, S. Ramazanov, T. Trčka, Brief Review of PVDF Properties and Applications Potential, Polymers 14 (2022) 4793. https://doi.org/10.3390/polym14224793.

[28] F. Orudzhev, D. Sobola, S. Ramazanov, K. Částková, N. Papež, D.A. Selimov, M. Abdurakhmanov, A. Shuaibov, A. Rabadanova, R. Gulakhmedov, V. Holcman, Piezo-Enhanced Photocatalytic Activity of the Electrospun Fibrous Magnetic PVDF/BiFeO3 Membrane, Polymers 15 (2023) 246. https://doi.org/10.3390/polym15010246.

[29] F. Latief, M. Absa, M. Andansari, M.A. Baqiya, S. Suasmoro, Synthesis of nano-size $BaTiO_3$ –$BiFeO_3$ system with low melting temperature KVO_3 addition, Ferroelectrics 599 (2022) 237–248. https://doi.org/10.1080/00150193.2022.2113655.

[30] D.E. Mazouzi, F. Djani, A. Soukeur, W. Bouchal, A. Manseri, K. Derkaoui, A. Martínez-Arias, A. Ksouri, F. Şen, M.M. Kaci, Auto-combustion designed BiFeO3/Bi2O3 photocatalyst for improved photodegradation of nitrobenzene under visible light and sunlight irradiation, Surfaces and Interfaces 44 (2024) 103581. https://doi.org/10.1016/j.surfin.2023.103581.

[31] X. Hu, X. Chen, M. Giagnorio, C. Wu, Y. Luo, C. Hélix-Nielsen, P. Yu, W. Zhang, Beaded electrospun polyvinylidene fluoride (PVDF) membranes for membrane distillation (MD), Journal of Membrane Science 661 (2022) 120850. https://doi.org/10.1016/j.memsci.2022.120850.

[32] A. Luraghi, F. Peri, L. Moroni, Electrospinning for drug delivery applications: A review, Journal of Controlled Release 334 (2021) 463–484. https://doi.org/10.1016/j.jconrel.2021.03.033.

[33] H. Zhang, X. Zhang, C. Qiu, P. Jia, F. An, L. Zhou, L. Zhu, D. Zhang, Polyaniline/ZnO heterostructure-based ammonia sensor self-powered by electrospinning of PTFE-PVDF/MXene piezo-tribo hybrid nanogenerator, Chemical Engineering Journal 496 (2024) 154226. https://doi.org/10.1016/j.cej.2024.154226.

[34] A.B. Rashid, M. Haque, S.M.M. Islam, K.M.R. Uddin Labib, Nanotechnology-enhanced fiber-reinforced polymer composites: Recent advancements on processing techniques and applications, Heliyon 10 (2024) e24692. https://doi.org/10.1016/j.heliyon.2024.e24692.

[35] R. Gayatri, A.N.S. Fizal, E. Yuliwati, M.S. Hossain, J. Jaafar, M. Zulkifli, W. Taweepreda, A.N. Ahmad Yahaya, Preparation and Characterization of PVDF–TiO2 Mixed-Matrix Membrane with PVP and PEG as Pore-Forming Agents for BSA Rejection, Nanomaterials 13 (2023) 1023. https://doi.org/10.3390/nano13061023.

[36] C. Salas, Solution electrospinning of nanofibers, in: Electrospun Nanofibers, Elsevier, 2017: pp. 73–108. https://doi.org/10.1016/B978-0-08-100907-9.00004-0.

[37] S. Bharathkumar, M. Sakar, Versatility of electrospinning on the fabrication of fibrous mat and mesh nanostructures of bismuth ferrite (BiFeO3) and their magnetic, photocatalytic activities, Phys. Chem. Chem. Phys., (2015). https://doi.org/10.1039/C5CP01640A.

[38] J. Zhang, Z. Jian, M. Jiang, B. Peng, Y. Zhang, Z. Wu, J. Zheng, Influence of Dispersed TiO2 Nanoparticles via Steric Interaction on the Antifouling Performance of PVDF/TiO2 Composite Membranes, Membranes 12 (2022) 1118. https://doi.org/10.3390/membranes12111118.

[39] A. Ichangi, K. Lê, A. Queraltó, M. Grosch, R. Weißing, F. Ünlü, A.K. Chijioke, A. Verma, T. Fischer, R. Surmenev, S. Mathur, Electrospun $BiFeO_3$ Nanofibers for Vibrational Energy Harvesting Application, Adv Eng Mater 24 (2022) 2101394. https://doi.org/10.1002/adem.202101394.

[40] C. Casut, I. Malaescu, C.N. Marin, M. Miclau, The Effect of Bi2O3 and Fe2O3 Impurity Phases in BiFeO3 Perovskite Materials on Some Electrical Properties in the Low-Frequency Field, Materials 15 (2022) 4764. https://doi.org/10.3390/ma15144764.

[41] U. Nuraini, S. Suasmoro, Crystal structure and phase transformation of $BiFeO_3$ multiferroics on the temperature variation, J. Phys.: Conf. Ser. 817 (2017) 012059. https://doi.org/10.1088/1742-6596/817/1/012059.

[42] X.H. Zheng, P.J. Chen, N. Ma, Z.H. Ma, D.P. Tang, Synthesis and dielectric properties of BiFeO3 derived from molten salt method, J Mater Sci: Mater Electron 23 (2012) 990–994. https://doi.org/10.1007/s10854-011-0533-4.

[43] J. Li, Q. Meng, W. Li, Z. Zhang, Influence of crystalline properties on the dielectric and energy storage properties of poly(vinylidene fluoride), J of Applied Polymer Sci 122 (2011) 1659–1668. https://doi.org/10.1002/app.34020.

[44] W. Li, Q. Meng, Y. Zheng, Z. Zhang, W. Xia, Z. Xu, Electric energy storage properties of poly(vinylidene fluoride), Applied Physics Letters 96 (2010) 192905. https://doi.org/10.1063/1.3428656.

[45] B.H. Arrosyid, A. Zulfi, S. Nur'aini, S. Hartati, A.F. Rafryanto, A. Noviyanto, D.A. Hapidin, D. Feriyanto, K. Khairurrijal, High-Efficiency Water Filtration by Electrospun Expanded Polystyrene Waste Nanofibers, ACS Omega 8 (2023) 23664–23672. https://doi.org/10.1021/acsomega.3c01718.

[46] R. Amalia, A. Noviyanto, L.A. Rahma, Merita, A. Labanni, M. Fahroji, S. Purwajanti, D.A. Hapidin, A. Zulfi, PVC waste-derived nanofiber: Simple fabrication with high potential performance for PM removal in air filtration, Sustainable Materials and Technologies 40 (2024) e00928. https://doi.org/10.1016/j.susmat.2024.e00928.

[47] F.H. Kusumah, S. Hartati, A. Noviyanto, A. Zulfi, N.T. Rochman, Optimasi Serat Selulosa Asetat/Gelatin/Ekstrak Bajakah (Spatholobus littoralis Hassk) menggunakan Pemintalan Elektrik, 8 (n.d.).

[48] S. Chauhan, M. Arora, P.C. Sati, S. Chhoker, S.C. Katyal, M. Kumar, Structural, vibrational, optical, magnetic and dielectric properties of Bi 1−x Ba x FeO 3 nanoparticles, Ceramics International 39 (2013) 6399–6405. https://doi.org/10.1016/j.ceramint.2013.01.066.

[49] Y. Wu, H. Zhang, Y. Xu, Z. Tang, Z. Li, Ferroelectric $BiFeO_3$ modified PVDF-based electrolytes for high-performance lithium metal batteries, J. Mater. Chem. A 12 (2024) 20403–20413. https://doi.org/10.1039/D4TA03225J.

[50] G. Magdy, A.H. Hassanin, I. Kandas, N. Shehata, PVDF nanostructures characterizations and techniques for enhanced piezoelectric response: A review, Materials Chemistry and Physics 325 (2024) 129760. https://doi.org/10.1016/j.matchemphys.2024.129760.

[51] G. Chang, X. Pan, Y. Hao, W. Du, S. Wang, Y. Zhou, J. Yang, Y. He, PVDF/ZnO piezoelectric nanofibers designed for monitoring of internal micro-pressure, RSC Adv. 14 (2024) 11775–11783. https://doi.org/10.1039/D3RA08713A.

[52] M. Koç, Effect of multilayer fabrication of PVDF/PZT fibers on output performance in piezoelectric nanogenerator (PEN), J Polym Res 31 (2024) 160. https://doi.org/10.1007/s10965-024-04004-5.

[53] E. Stojchevska, P. Makreski, M. Zanoni, L. Gasperini, G. Selleri, D. Fabiani, C. Gualandi, A. Bužarovska, Piezoelectric PVDF-TrFE nanocomposite mats filled with $BaTiO_3$ nanofibers: The effect of poling conditions, Polymers for Advanced Techs 35 (2024) e6333. https://doi.org/10.1002/pat.6333.